Proceedings of the ASME 2025
Aerospace Structures, Structural Dynamics, and Materials Conference
SSDM2025
May 5-7, 2025, Houston, Texas

SSDM2025-152404

FATIGUE PERFORMANCE ASSESSMENT OF AUXETIC LATTICE STRUCTURES

Serhat Arda Şahin[1], İnci Pir[1,*], Mertol Tüfekci[2,3], Ekrem Tüfekci[1]

[1] Faculty of Mechanical Engineering, Istanbul Technical University
Istanbul, Turkey
[2] Center for Engineering Research, University of Hertfordshire
Hertfordshire, United Kingdom
[3] School of Physics, Engineering and Computer Science, University of Hertfordshire, Hatfield,
Hertfordshire AL10 9AB, UK
*Correspondance: İnci Pir, pirin@itu.edu.tr

ABSTRACT

Lattice structures, widely utilised in aerospace and automotive applications, offer high strength-to-weight ratios, particularly when optimised through additive manufacturing. This study evaluates the fatigue performance of four auxetic lattice structures fabricated from Ti-6Al-4V alloy. The geometries were designed with consistent dimensions and analysed in single and 3x3 multi-cell configurations under fixed support and symmetric loading conditions. Structural simulations were conducted using Ansys Workbench, where tensile forces of 10 MPa and 20 MPa were applied to single and multi-cell models, respectively. Results reveal that Auxetic 3 exhibited the longest fatigue life (5.66 million cycles) due to smooth transitions and uniform stress distribution, while Auxetic 2 displayed the shortest fatigue life (233,040 cycles) owing to significant localised stress concentrations. A comparison of single and multi-cell models demonstrated that stress accumulation at cell connections in multi-cell structures reduces overall fatigue life. These findings provide a basis for finding better auxetic lattice structures for enhanced durability in load-bearing applications.

Keywords: Lattice structures, 3D printing, Fatigue, Finite element method, Ti-6Al-4V

NOMENCLATURE

3x3 Multi-cell	Multi-cell lattice configuration
°C	Degree Celcius
mm³	Cubic millimetre
MPa	Megapascal
S-N Curve	Stress-Cycle Fatigue Curve
Ti-6Al-4V	Material alloy: Titanium-6%Al-4%V
LPBF	Laser Powder Bed Fusion
DED	Direct Energy Deposition
FEA	Finite Element Analysis
S-N	Stress-Life
HCF	High-Cycle Fatigue
ε-N	Strain-Life
LCF	Low-Cycle Fatigue

1. INTRODUCTION

Lattice structures, categorised as a unique type of metamaterial, are constructed through the tessellation of periodic unit cells to manifest distinct macro-scale properties and behaviours. These designs have seen an increase in research interest propelled by advancements in additive manufacturing technologies [1], [2]. Traditionally difficult to fabricate via conventional methods, such structures often mirror natural patterns such as hexagonal lattices known for their stiffness, resilience, and energy absorption capabilities [3], [4], [5], [6]. These characteristics are vital for achieving an optimal stiffness-to-weight ratio, a common objective in numerous engineering fields [7], [8].

Recent developments have broadened the application of metamaterials, introducing new classes of two-dimensional structural metamaterials with curved elements in their unit cells to enhance mechanical properties and application versatility in areas ranging from bioengineering to stretchable electronics and impact absorbers [9], [10], [11]. The geometric configurations of these lattice structures significantly influence their mechanical behaviour [18,19]. In aerospace applications, for example, these materials are ranked for their specific stiffness and low density, essential for components like airframes and rotor blades [12], [13], [14], [15], [16]. Research has been focused on refining the elastic moduli of both regular and irregular hexagonal lattice materials to improve structural stiffness [17].

The selection of materials and control over the manufacturing processes are crucial when utilising additive manufacturing techniques such as Fused Deposition Modelling (FDM). This method involves extruding thermoplastic filaments through a heated nozzle, building the structure layer by layer [18], [19]. The mechanical integrity of the structures is significantly influenced by the control of nozzle temperature and the trajectory defined by the slicing software, along with other key printing parameters like temperature settings and layer height [20], [21].

Optimising the FDM process is crucial for efficiently replicating lattice structures without compromising mechanical properties or structural integrity [22], [23], [24]. The choice of infill patterns, such as concentric, honeycomb, and rectilinear, affects the lattice's weight, strength, stiffness, and printing duration [25], [26]. Previous studies indicate that while rectilinear patterns with full infill density yield higher tensile strength, honeycomb patterns exhibit superior tensile strength at lower densities. However, this advantage diminishes as infill density increases [25]. Fatigue behaviour examination of samples is also an important issue [27], [28]. The fatigue behaviour of 3D-printed structures depends significantly on infill geometry, offering superior fatigue resistance due to uniform stress distribution and reduced stress concentration [29]. Higher infill density and smoother, continuous geometries enhance fatigue life, making them ideal for load-bearing applications [30], [31].

The present study evaluates the fatigue performance of four distinct auxetic lattice structures designed with consistent geometric dimensions to ensure comparability. Single-cell and 3x3 multi-cell configurations were considered to investigate the influence of lattice geometry and cell connectivity on fatigue behaviour [32], [33], [34]. Numerical simulations were conducted using Ansys Workbench with Ti-6Al-4V, a titanium alloy widely used in aerospace and additive manufacturing applications, as the material. Tensile forces were applied to simulate operational stress conditions, and fatigue life was assessed through cyclic loading analysis. This study aims to identify the better auxetic lattice structure with enhanced fatigue performance, offering valuable insights for their application in lightweight, load-bearing components.

2. MATERIALS AND METHODS

In this study, four different auxetic lattice structures were investigated. The geometries of these structures were designed according to the guidelines given in [9], [10], [11]. The primary consideration in designing these geometries was to ensure that the unit cells of each structure were comparable by maintaining similar geometric dimensions. Accordingly, the volumes of the single cells were set at 1330 mm³, while the volumes of the multiple cells were set at 18,000 mm³. This volume for the multiple cells was chosen because a multiple cell contains approximately 14 single cells, making 18,000 mm³ a reasonable value. When designing the multi-cell structures, the cells were arranged in a 3-2-3 pattern from top to bottom. The investigated lattice structures are displayed in Figure 1.

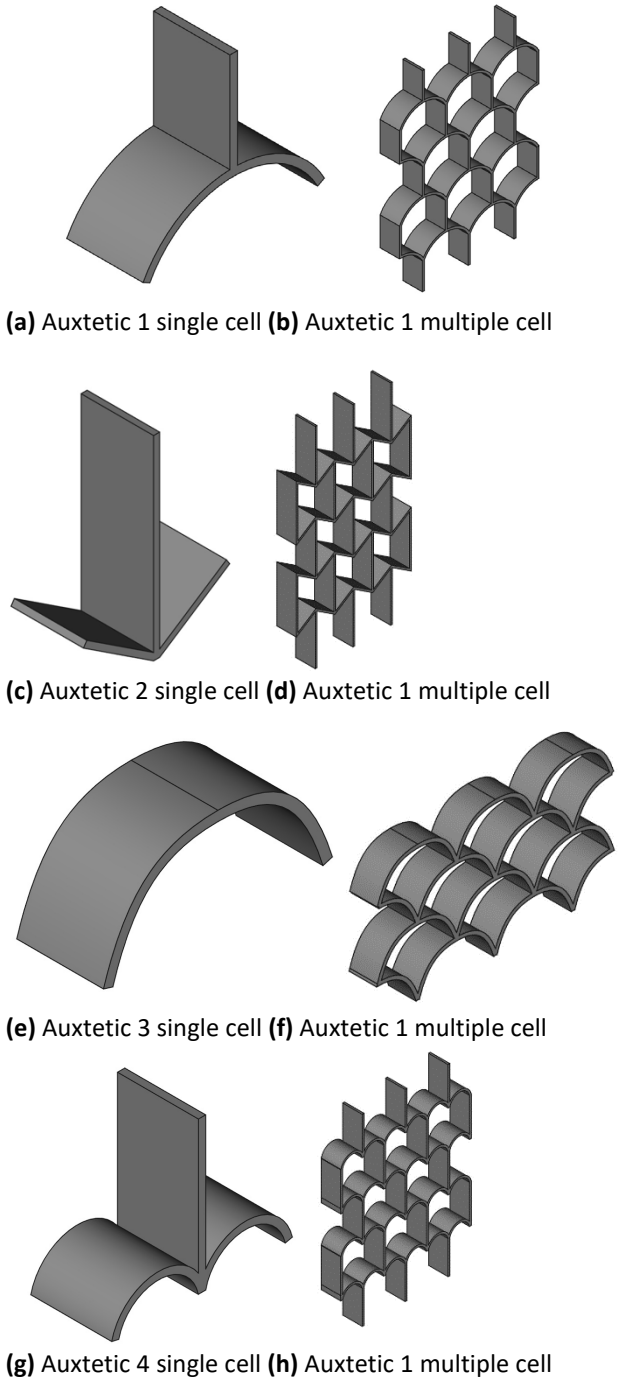

(a) Auxtetic 1 single cell **(b)** Auxtetic 1 multiple cell

(c) Auxtetic 2 single cell **(d)** Auxtetic 1 multiple cell

(e) Auxtetic 3 single cell **(f)** Auxtetic 1 multiple cell

(g) Auxtetic 4 single cell **(h)** Auxtetic 1 multiple cell

FIGURE 1: LATTICE STRUCTURES INVESTIGATED

Once the designs had been completed, structural analysis modelling was initiated using Ansys Workbench with the objective of solving the systems and comparing the results. The initial stage of the modelling process was selecting the appropriate material. As previously stipulated, Ti-6Al-4V was selected as the material. Ti-6Al-4V is a titanium alloy that is widely utilised in a number of industries, including aerospace,

automotive, medical and energy. The alloy consists of 90% titanium, 6% aluminium, and 4% vanadium. This alloy is particularly suitable for 3D printing technologies, such as Laser Powder Bed Fusion (LPBF) and Direct Energy Deposition (DED), due to its high melting point and low thermal conductivity, which facilitate precise part production. Furthermore, its mechanical properties can be tailored as needed, and its lightweight nature makes it advantageous for additive manufacturing applications. The mechanical properties of the material used in this study are shown in Figure 2.

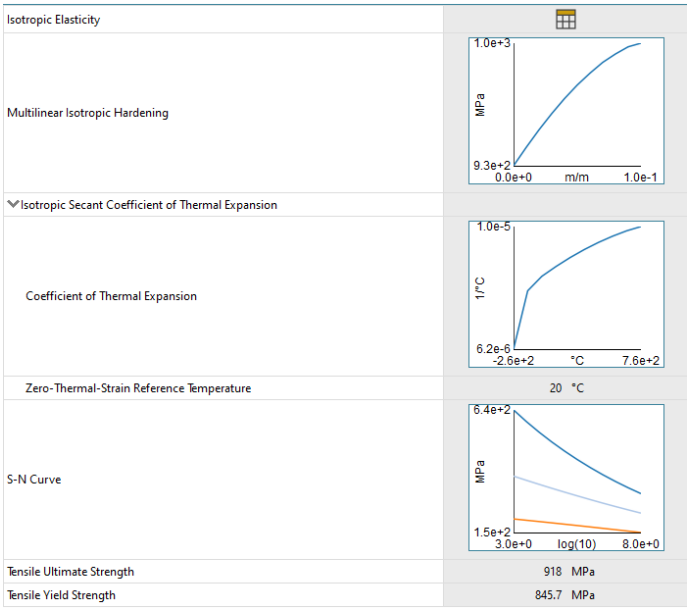

FIGURE 2: MECHANICAL PROPERTIES OF TI-6AL-4V FROM ANSYS WORKBENCH

The same approach was followed for all models, whereby the geometry was constrained in the 1-2-3 degrees of freedom, and the 4-5-6 degrees of freedom were left free. The applied boundary conditions to single and multiple-cell models are given in Figures 3 and 4. The mesh structure was standardised across all models.

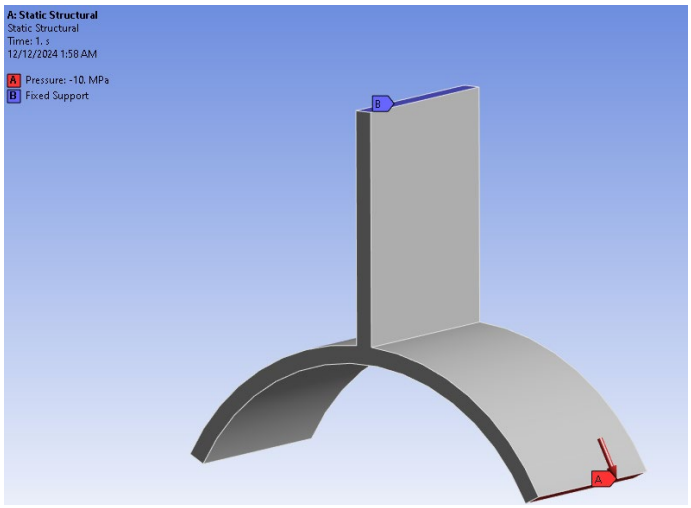

FIGURE 3: BOUNDARY CONDITIONS OF AUXETIC 1 SINGLE CELL LATTICE STRUCTURE

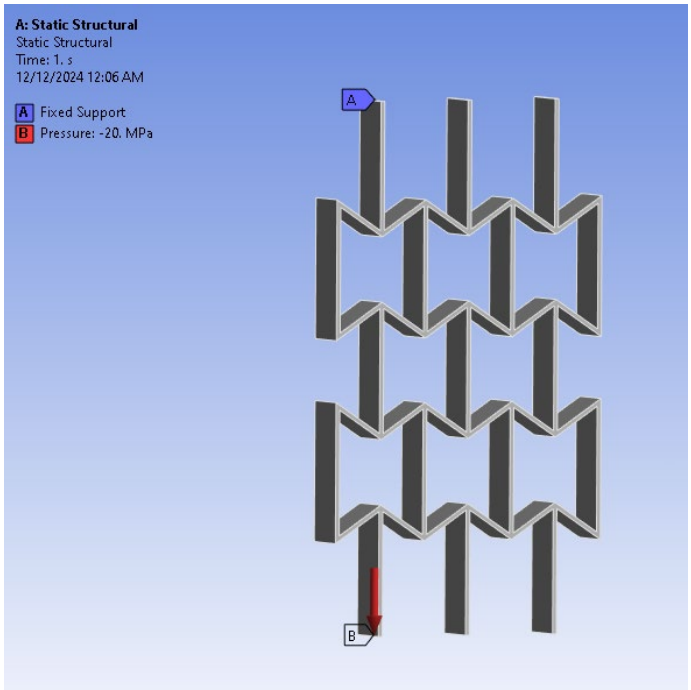

FIGURE 4: BOUNDRY CONDITIONS OF AUXETIC 2 MULTIPLE LATTICE STRUCTURE

The Ansys Workbench software was employed to define the mesh type as "Sweep," set the element size to 1 mm, and ensure that there was a minimum of two elements along each edge. While constructing the mesh model, mesh convergence studies were considered. Subsequently, models were created in which tensile forces were applied to both single and multiple lattice structures following the completion of the meshing process. The tensile force was defined as a pressure applied to a specific area, with values set at 10 MPa for single cells and 20 MPa for multiple cells. These values were selected to induce approximately half of the material's strength in stress, facilitating

clearer insights into the fatigue life in subsequent fatigue analyses. Applied loads to the models are given as a table in Table 1. Constant stress amplitude is applied to the models between "-1 and 1". The solution scheme is summarised and given in Figure 5, and the stress amplitude graph is detailed in Figure 6.

TABLE 1: APPLIED SURFACE TRACTION VALUES FOR EACH MODEL

Single Lattice Structure	10 MPa applied
Multiple Lattice Structure	20 MPa applied

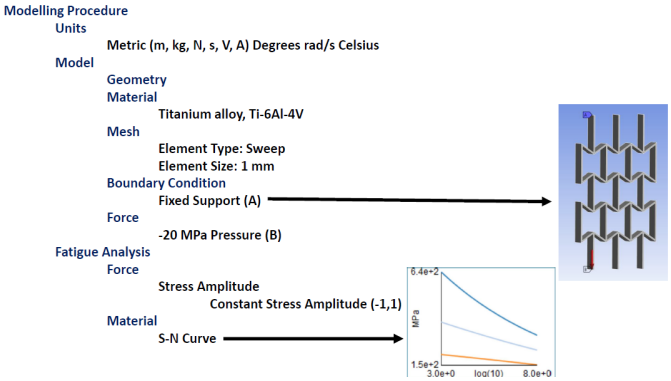

FIGURE 5: SOLUTION SCHEME

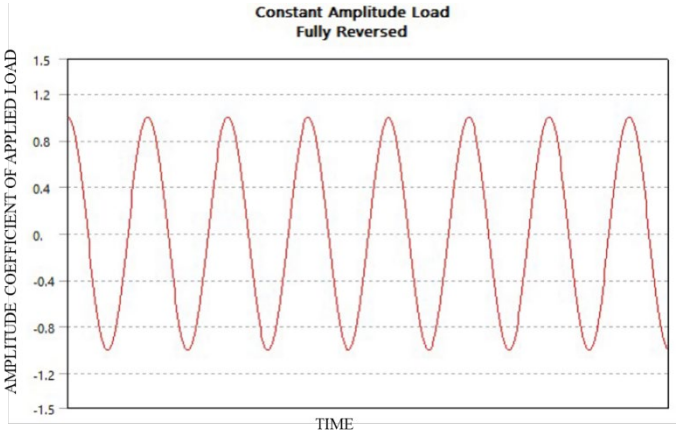

FIGURE 6: STRESS AMPLITUDE GRAPH FOLLOWED IN THE STUDY

The tensile analysis data obtained were processed using the "Fatigue Tool" in Ansys Workbench to evaluate the fatigue life of the structures. The Ansys Fatigue Tool is a specialised module within Ansys software designed to predict the lifespan of samples subjected to cyclic loading. It evaluates fatigue failure using stress or strain data from Finite Element Analysis (FEA) and applies fatigue theories to estimate the number of cycles to failure. This tool follows a structured workflow, starting with the import of FEA results, followed by the identification of load cycles, and the application of fatigue models. Two primary approaches are used within this tool. The first one is the Stress-Life (S-N) method, which is suitable for High-Cycle Fatigue (HCF) where stresses remain below the yield strength, and the second one is the Strain-Life (ε-N) method, which is used for Low-Cycle Fatigue (LCF) where plastic deformation occurs. By integrating finite element stress analysis with established fatigue models, the Ansys Fatigue Tool provides a comprehensive approach for determining the fatigue behaviour of the sample under complex cyclic loading conditions. The results and discussions section presents a comparative analysis of the fatigue life of the different geometries.

3. RESULTS AND DISCUSSION

It is essential to assess the mechanical performance of lattice structures in conjunction with their material properties. In addition to the geometric design, the mechanical properties of the material have a significant impact on the fatigue life, maximum stress, and deformation. The data indicate that the material has a tensile ultimate strength of 918 MPa and a tensile yield strength of 845.7 MPa. These properties are of critical importance with regard to the material's mechanical durability and functionality. This study is comprised of two principal phases. The initial stage comprises an examination of multi-cell geometries, followed by an analysis of single-cell structures.

The analysis of multi-cell structures revealed that the Auxetic 1 structure exhibited the highest maximum stress value (397.48 MPa) and total deformation value (0.96 mm) among the four structures. It exhibits the second-lowest stress value among the four lattice structures. The fatigue life of Auxetic 1 was found to be 1,660,000 cycles. It was observed that, in contrast to the maximum stress value, this fatigue life is inversely proportional and is the second highest among the four lattice structures.

The maximum stress value for the Auxetic 2 structure is 450.45 MPa, with a total deformation value of 0.84 mm. It exhibits the highest stress value among the four lattice structures. It can be surmised that the Auxetic 2 structure is prone to localised stress concentrations, particularly when subjected to tensile stress, rendering it less favourable in comparison to the other three structures. The fatigue life of Auxetic 2 is 233,040 cycles. As the maximum stress value on the geometry increases, the fatigue life decreases, as was observed previously. It can thus be concluded that Auxetic 2 has the shortest fatigue life of the four geometries. A representative result of the multiple-cell lattice structure analysis of Auxetic 2 multiple cell is given in Figure 7.

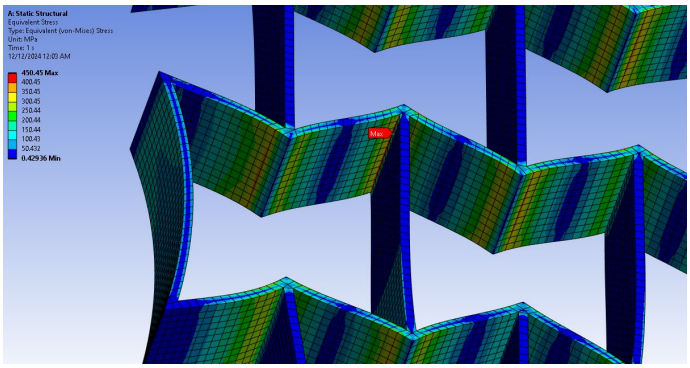

FIGURE 7: MAX STRESS LOCATION OF AUXETIC 2 MULTIPLE CELL

In contrast, Auxetic 3 exhibits a maximum stress value of 368.05 MPa and a total deformation value of 0.87 mm, representing the lowest stress value among the four lattice structures. This indicates that Auxetic 3 does not induce local stress concentrations, which contributes to its highest fatigue life of 5,660,000 cycles. Maximum stress and equivalent elastic strain results of Auxetic 3 multiple cell are given in Figure 8.

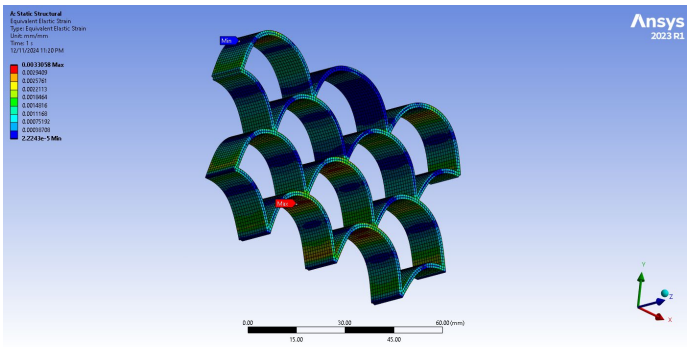

(a) Equivalent elastic strain of Auxtetic 3 multiple cell

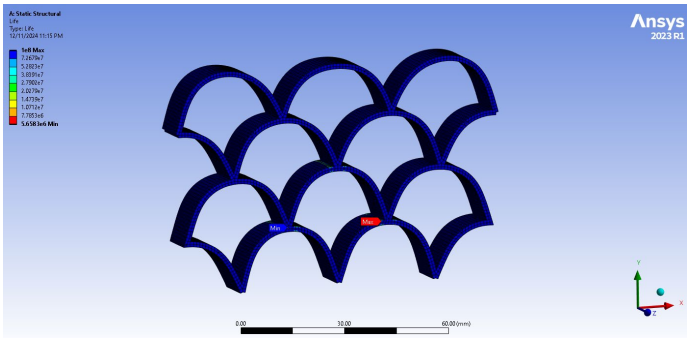

(b) Fatigue life of Auxtetic 3 multiple cell

FIGURE 8: MAX STRESS AND FATIGUE ANALYSIS RESULTS OF AUXETIC 3

Similar to Auxetic 2, Auxetic 4 permitted the occurrence of multiple stress concentrations, resulting in a maximum stress value of 408.56 MPa. Given that it has the second-highest stress value in the list, it can be concluded that it has a low fatigue life. The analysis demonstrated that Auxetic 4 has a fatigue life of 1,080,000 cycles. In conclusion, it has been observed that the maximum stress value on the geometry significantly affects the fatigue life. Among the four different auxetic geometries, Auxetic 3 has the lowest stress value due to its smoother transitions and connections, which lead to a more homogeneous distribution of stress. In contrast, Auxetic 2 has sharp transitions, which cause local stress concentrations and result in a shorter fatigue life. Figures 7 and 8 are representative results of the multiple-cell lattice structure analysis; meanwhile, in Table 2, the lifetime cycles and in Table 3, the maximum stress and deformation results of evaluated models are summarised.

TABLE 2: FATIGUE LIFETIMES OF MULTIPLE CELL LATTICE STRUCTURES

Lattice Structure(Multiple)	Fatigue Lifetime(cycles)
Auxtetic 1	1.66E+06
Auxtetic 2	2.33E+05
Auxtetic 3	5.66E+06
Auxtetic 4	1.08E+06

TABLE 3: MAXIMUM STRESS AND TOTAL DEFORMATION RESULTS OF MULTIPLE CELL LATTICE STRUCTURES

Lattice Structure (Multiple)	Maximum Stress (MPa)	Total Deformation (mm)
Auxtetic 1	397.78	0.96125
Auxtetic 2	450.45	0.83588
Auxtetic 3	368.05	0.87195
Auxtetic 4	408.56	1.0097

In Figures 9 and 10, the fatigue strength comparisons of each model are given.

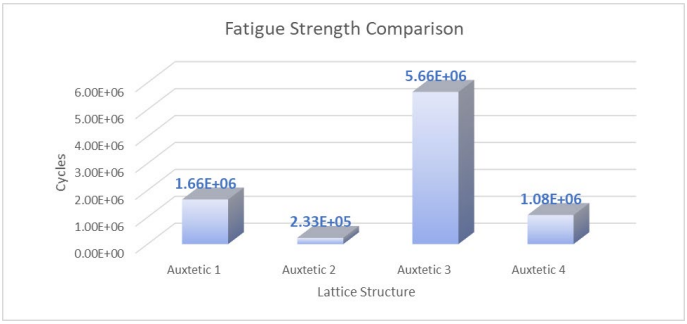

FIGURE 9: FATIGUE STRENGTH COMPARISON OF MULTIPLE MODELS

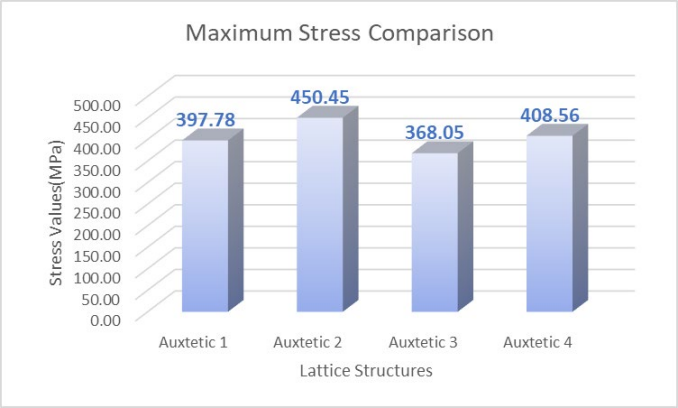

FIGURE 10: MAXIMUM STRESS COMPARISON OF MULTIPLE MODELS

The second step will entail an examination of the analysis results pertaining to single-cell structures, with a view to ascertaining whether any analogy can be drawn between them and multi-cell structures.

The Auxetic 1 structure exhibits a maximum stress of 360.98 MPa and a total deformation of 0.4 mm. The level of stress and deformation exhibited by this structure is moderate in comparison to the other structures. The fatigue life of the structure is found to be 7.67E+06 cycles, which makes it the second most durable structure in terms of fatigue life. Although the maximum stress is not the highest, the structure demonstrates a relatively good fatigue life due to its overall design.

The Auxetic 2 structure exhibits the highest resilience in terms of deformation, with a maximum stress of 17.44 MPa and a total deformation of 0.0047 mm. Despite exhibiting minimal deformation, Auxetic 2 exhibits the longest fatigue life at 1.08E+08 cycles. This indicates that the structure displays high resistance to cyclic loading, as the low-stress value suggests that it does not experience significant stress concentrations, thereby increasing its fatigue resistance. It can thus be posited that Auxetic 2 represents the better structure for long-term durability among the ones investigated.

Auxetic 3 exhibits a higher maximum stress of 440.92 MPa and a total deformation of 0.64 mm, which is relatively high in comparison to the other structures. The fatigue life of this structure is 3.24E+05 cycles, which is considerably lower than that of Auxetic 2. This indicates that although the structure can withstand relatively high stress, its fatigue life is adversely affected by this higher stress, resulting in an earlier failure under cyclic loading. Maximum stress and equivalent elastic strain results of auxetic 3 single cell are given in Figure 11.

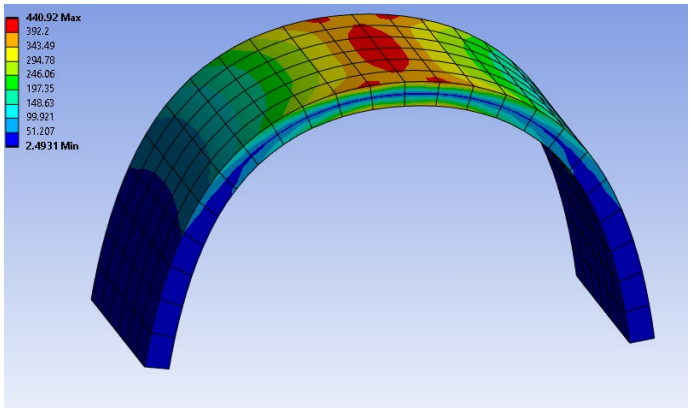

(a) Equivalent elastic strain of Auxtetic 3 single cell

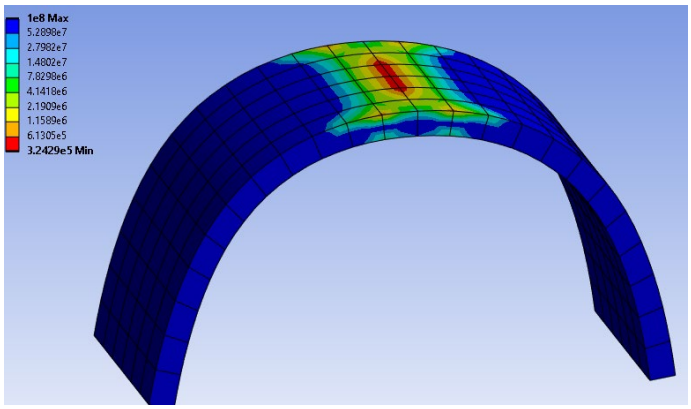

(b) Fatigue life of Auxtetic 3 single cell

FIGURE 11: MAX STRESS AND FATIGUE ANALYSIS RESULTS OF AUXETIC 3 SINGLE

The highest maximum stress of 605.25 MPa and the same total deformation of 0.64 mm exhibited by Auxetic 4, indicate that this structure has the shortest fatigue life of all four structures, at 2258.8 cycles. The elevated stress value and the comparatively high deformation indicate that this structure is subjected to considerable localised stress concentrations, which markedly diminish its fatigue resistance. It can thus be concluded that Auxetic 4 is less suitable for applications requiring high durability and low failure rates.

A comparison of the two studies reveals that the results differ significantly between single-cell and multi-cell structures. This suggests that stress accumulation occurs at the points where single cells connect when transitioning into multi-cell structures. Consequently, it can be recommended that future processes, analyses and operations should be performed on multi-cell structures when designing these geometries. Figure 11 displays the fatigue life and the maximum stress plots of Auxetic 3 single cell lattice structure whilst, in Table 4, the lifetime cycles and in Table 5, the maximum stress and deformation results of evaluated models are summarised for single-cell cases.

TABLE 4: FATIGUE LIFETIMES OF EACH LATTICE STRUCTURE

Lattice Structure(Single)	Fatigue lifetime (cycles)
Auxtetic 1	7.67E+06
Auxtetic 2	1.08E+08
Auxtetic 3	3.24E+05
Auxtetic 4	2258.8

TABLE 5: MAXIMUM STRESS AND TOTAL DEFORMATION RESULTS

Lattice Structure (Single)	Maximum Stress (MPa)	Total Deformation (mm)
Auxtetic 1	360.98	0.4
Auxtetic 2	17.44	0.0047
Auxtetic 3	440.92	0.64
Auxtetic 4	605.25	0.64

In Figures 12 and 13, the fatigue strength comparisons of each model are given.

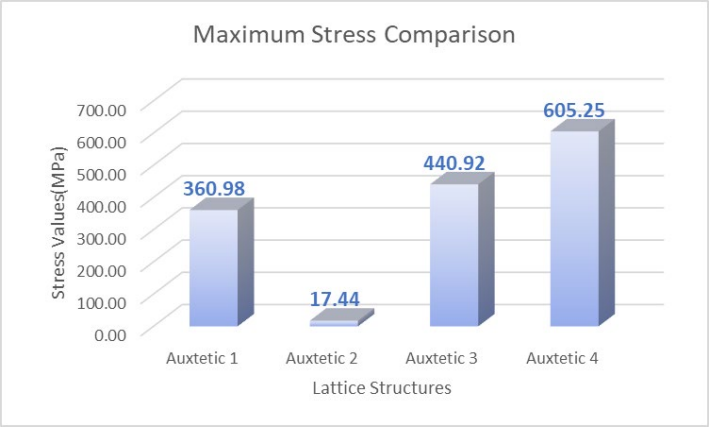

FIGURE 12: MAXIMUM STRESS COMPARISON OF SINGLE MODELS

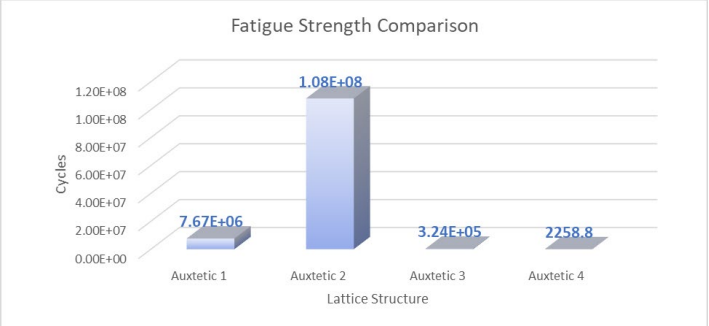

FIGURE 13: FATIGUE STRENGTH COMPARISON OF SINGLE MODELS

4. CONCLUSION

In this study, the fatigue performance of four auxetic lattice structures was evaluated using numerical simulations. Single-cell and 3x3 multi-cell configurations were designed with consistent geometric dimensions to ensure comparability. The Ti-6Al-4V alloy, widely utilised in additive manufacturing, was selected as the material for analysis. Tensile forces were applied under fixed boundary conditions to simulate operational stresses, and the fatigue life of each structure was assessed using the Ansys Workbench Fatigue Tool.

The results revealed that the geometry of the lattice structures plays a significant role in their fatigue behaviour. Auxetic 3 demonstrated the longest fatigue life due to its smooth transitions and uniform stress distribution, while Auxetic 2 exhibited the shortest fatigue life as a result of localised stress concentrations. Furthermore, multi-cell configurations experienced additional stress accumulations at the connections between cells, reducing their fatigue life compared to single-cell models. These findings highlight the importance of geometric continuity and uniform stress distribution in improving the performance of auxetic structures.

For future work, experimental validation of these results is recommended through physical testing of 3D-printed lattice structures using additive manufacturing techniques. Investigating the effects of alternative materials, dynamic loading conditions, and varying boundary constraints could provide further insights. Additionally, extending the study to larger, more complex multi-cell configurations and exploring new lattice geometries will enhance the applicability of these findings in real-world load-bearing components.

REFERENCES

[1] A. Srivastava, "Elastic metamaterials and dynamic homogenization: a review," *Int. J. Smart Nano Mater.*, vol. 6, no. 1, pp. 41–60, Jan. 2015, doi: 10.1080/19475411.2015.1017779.

[2] J. T. Costa, M. G. Silveirinha, and S. I. Maslovski, "Finite-difference frequency-domain method for the extraction of effective parameters of metamaterials," *Phys. Rev. B*, vol. 80, no. 23, p. 235124, Dec. 2009, doi: 10.1103/PhysRevB.80.235124.

[3] U. M. Dilberoglu, B. Gharehpapagh, U. Yaman, and M. Dolen, "The Role of Additive Manufacturing in the Era of Industry 4.0," *Procedia Manuf.*, vol. 11, pp. 545–554, 2017, doi: 10.1016/j.promfg.2017.07.148.

[4] C. H. Lee, F. N. B. M. Padzil, S. H. Lee, Z. M. A. Ainun, and L. C. Abdullah, "Potential for Natural Fiber Reinforcement in PLA Polymer Filaments for Fused Deposition Modeling (FDM) Additive Manufacturing: A Review," *Polymers (Basel).*, vol. 13, no. 9, p. 1407, Apr. 2021, doi: 10.3390/polym13091407.

[5] S. Marimuthu *et al.*, "Finite element modelling of substrate thermal distortion in direct laser additive manufacture of an aero-engine component," *Proc. Inst.*

Mech. Eng. Part C J. Mech. Eng. Sci., vol. 227, no. 9, pp. 1987–1999, Sep. 2013, doi: 10.1177/0954406212470363.

[6] V. Öztekin and Ş. Yılmaz, "Experimental and Numerical Investigation of the Gurson–Tveergard–Needleman Model Parameters for AISI 1045 Steel," *steel Res. Int.*, vol. 94, no. 6, Jun. 2023, doi: 10.1002/srin.202200785.

[7] C. Talischi, G. H. Paulino, and C. H. Le, "Honeycomb Wachspress finite elements for structural topology optimization," *Struct. Multidiscip. Optim.*, vol. 37, no. 6, pp. 569–583, Feb. 2009, doi: 10.1007/s00158-008-0261-4.

[8] I. Maskery and I. A. Ashcroft, "The deformation and elastic anisotropy of a new gyroid-based honeycomb made by laser sintering," *Addit. Manuf.*, vol. 36, p. 101548, Dec. 2020, doi: 10.1016/j.addma.2020.101548.

[9] S. Mukherjee and S. Adhikari, "The in-plane mechanics of a family of curved 2D lattices," *Compos. Struct.*, vol. 280, p. 114859, Jan. 2022, doi: 10.1016/j.compstruct.2021.114859.

[10] T. Mukhopadhyay, S. Adhikari, and A. Batou, "Frequency domain homogenization for the viscoelastic properties of spatially correlated quasi-periodic lattices," *Int. J. Mech. Sci.*, vol. 150, pp. 784–806, Jan. 2019, doi: 10.1016/j.ijmecsci.2017.09.004.

[11] S. Adhikari, T. Mukhopadhyay, and X. Liu, "Broadband dynamic elastic moduli of honeycomb lattice materials: A generalized analytical approach," *Mech. Mater.*, vol. 157, p. 103796, Jun. 2021, doi: 10.1016/j.mechmat.2021.103796.

[12] J. Plocher and A. Panesar, "Effect of density and unit cell size grading on the stiffness and energy absorption of short fibre-reinforced functionally graded lattice structures," *Addit. Manuf.*, vol. 33, p. 101171, May 2020, doi: 10.1016/j.addma.2020.101171.

[13] A. Schmitz and P. Horst, "A finite element unit-cell method for homogenised mechanical properties of heterogeneous plates," *Compos. Part A Appl. Sci. Manuf.*, vol. 61, pp. 23–32, Jun. 2014, doi: 10.1016/j.compositesa.2014.01.014.

[14] H. J. Böhm and W. Han, "Comparisons between three-dimensional and two-dimensional multi-particle unit cell models for particle reinforced metal matrix composites," *Model. Simul. Mater. Sci. Eng.*, vol. 9, no. 2, pp. 47–65, Mar. 2001, doi: 10.1088/0965-0393/9/2/301.

[15] T. Okabe, M. Nishikawa, and H. Toyoshima, "A periodic unit-cell simulation of fiber arrangement dependence on the transverse tensile failure in unidirectional carbon fiber reinforced composites," *Int. J. Solids Struct.*, vol. 48, no. 20, pp. 2948–2959, Oct. 2011, doi: 10.1016/j.ijsolstr.2011.06.012.

[16] Y. Fu and W. Liu, "Design of mechanical metamaterial with controllable stiffness using curved beam unit cells," *Compos. Struct.*, vol. 258, p. 113195, Feb. 2021, doi: 10.1016/j.compstruct.2020.113195.

[17] J. Zeman, R. H. J. Peerlings, and M. G. D. Geers, "Non-local energetics of random heterogeneous lattices," *J. Mech. Phys. Solids*, vol. 59, no. 6, pp. 1214–1230, Jun. 2011, doi: 10.1016/j.jmps.2011.03.006.

[18] C. Ziemian, M. Sharma, and S. Ziemi, "Anisotropic Mechanical Properties of ABS Parts Fabricated by Fused Deposition Modelling," in *Mechanical Engineering*, InTech, 2012. doi: 10.5772/34233.

[19] J. M. Chacón, M. A. Caminero, P. J. Núñez, E. García-Plaza, I. García-Moreno, and J. M. Reverte, "Additive manufacturing of continuous fibre reinforced thermoplastic composites using fused deposition modelling: Effect of process parameters on mechanical properties," *Compos. Sci. Technol.*, vol. 181, p. 107688, Sep. 2019, doi: 10.1016/j.compscitech.2019.107688.

[20] A. Chadha, M. I. Ul Haq, A. Raina, R. R. Singh, N. B. Penumarti, and M. S. Bishnoi, "Effect of fused deposition modelling process parameters on mechanical properties of 3D printed parts," *World J. Eng.*, vol. 16, no. 4, pp. 550–559, Jul. 2019, doi: 10.1108/WJE-09-2018-0329.

[21] A. K. Sood, R. K. Ohdar, and S. S. Mahapatra, "Parametric appraisal of mechanical property of fused deposition modelling processed parts," *Mater. Des.*, vol. 31, no. 1, pp. 287–295, Jan. 2010, doi: 10.1016/j.matdes.2009.06.016.

[22] X. Wang, M. Jiang, Z. Zhou, J. Gou, and D. Hui, "3D printing of polymer matrix composites: A review and prospective," *Compos. Part B Eng.*, vol. 110, pp. 442–458, Feb. 2017, doi: 10.1016/j.compositesb.2016.11.034.

[23] R. Roy, S.-J. Park, J.-H. Kweon, and J.-H. Choi, "Characterization of Nomex honeycomb core constituent material mechanical properties," *Compos. Struct.*, vol. 117, pp. 255–266, Nov. 2014, doi: 10.1016/j.compstruct.2014.06.033.

[24] C. Pascual-González, M. Iragi, A. Fernández, J. P. Fernández-Blázquez, L. Aretxabaleta, and C. S. Lopes, "An approach to analyse the factors behind the micromechanical response of 3D-printed composites," *Compos. Part B Eng.*, vol. 186, p. 107820, Apr. 2020, doi: 10.1016/j.compositesb.2020.107820.

[25] S. A. Khan, B. A. Siddiqui, M. Fahad, and M. A. Khan, "Evaluation of the Effect of Infill Pattern on Mechanical Stregnth of Additively Manufactured Specimen," *Mater. Sci. Forum*, vol. 887, pp. 128–132, Mar. 2017, doi: 10.4028/www.scientific.net/MSF.887.128.

[26] K. Wang, X. Xie, J. Wang, A. Zhao, Y. Peng, and Y. Rao, "Effects of infill characteristics and strain rate on the deformation and failure properties of additively manufactured polyamide-based composite structures," *Results Phys.*, vol. 18, p. 103346, Sep. 2020, doi: 10.1016/j.rinp.2020.103346.

[27] R. Jones, A. J. Kinloch, J. G. Michopoulos, A. J. Brunner, and N. Phan, "Delamination growth in polymer-matrix fibre composites and the use of fracture mechanics data for material characterisation and life

prediction," *Compos. Struct.*, vol. 180, pp. 316–333, Nov. 2017, doi: 10.1016/j.compstruct.2017.07.097.
[28] S. Michel, A. J. Kinloch, and R. Jones, "Cyclic-fatigue crack growth in polymer composites: Data interpretation via the Hartman-Schijve methodology," *Eng. Fract. Mech.*, p. 110743, Dec. 2024, doi: 10.1016/j.engfracmech.2024.110743.
[29] H. Bakhtiari, M. Aamir, and M. Tolouei-Rad, "Effect of 3D Printing Parameters on the Fatigue Properties of Parts Manufactured by Fused Filament Fabrication: A Review," *Appl. Sci.*, vol. 13, no. 2, p. 904, Jan. 2023, doi: 10.3390/app13020904.
[30] M. C. Dudescu, L. Racz, and F. Popa, "Effect of infill pattern on fatigue characteristics of 3D printed polymers," *Mater. Today Proc.*, vol. 78, pp. 263–269, 2023, doi: 10.1016/j.matpr.2022.11.283.
[31] M. Qamar Tanveer, G. Mishra, S. Mishra, and R. Sharma, "Effect of infill pattern and infill density on mechanical behaviour of FDM 3D printed Parts- a current review," *Mater. Today Proc.*, vol. 62, pp. 100–108, 2022, doi: 10.1016/j.matpr.2022.02.310.
[32] M. Tüfekci, "Performance evaluation analysis of Ti-6Al-4V foam fan blades in aircraft engines: A numerical study," *Compos. Part C Open Access*, vol. 12, p. 100414, Oct. 2023, doi: 10.1016/j.jcomc.2023.100414.
[33] M. Tüfekci *et al.*, "Low strain rate mechanical performance of balsa wood and carbon fibre-epoxy-balsa sandwich structures," *Compos. Part C Open Access*, vol. 12, p. 100416, Oct. 2023, doi: 10.1016/j.jcomc.2023.100416.
[34] L. Yao, R. C. Alderliesten, R. Jones, and A. J. Kinloch, "Delamination fatigue growth in polymer-matrix fibre composites: A methodology for determining the design and lifing allowables," *Compos. Struct.*, vol. 196, pp. 8–20, Jul. 2018, doi: 10.1016/j.compstruct.2018.04.069.

